Journal of Quantitative Spectroscopy & Radiative Transfer 215 (2018) 9–12

Contents lists available at ScienceDirect

Journal of Quantitative Spectroscopy & Radiative Transfer

journal homepage: www.elsevier.com/locate/jqsrt

Extended sub-Doppler resolution spectroscopy of the ν_3 band of methane

Philip A. Kocheril[a], Charles R. Markus[a], Anne Marie Esposito[a], Alex W. Schrader[a], Thomas S. Dieter[b,1], Benjamin J. McCall[a,b,c,*]

[a] Department of Chemistry, University of Illinois at Urbana-Champaign, Urbana, IL 61801, USA
[b] Department of Physics, University of Illinois at Urbana-Champaign, Urbana, IL 61801, USA
[c] Department of Astronomy, University of Illinois at Urbana-Champaign, Urbana, IL 61801, USA

ARTICLE INFO

Article history:
Received 5 April 2018
Revised 29 April 2018
Accepted 30 April 2018
Available online 30 April 2018

Keywords:
Methane
Mid-infrared
Sub-Doppler

ABSTRACT

We have performed sub-Doppler resolution rovibrational spectroscopy of the ν_3 band of methane ($^{12}CH_4$) in the mid-infrared using an optical parametric oscillator in a double-pass configuration for saturated absorption. An optical frequency comb was used for absolute frequency calibration. We have measured 22 methane line centers ranging from the $P(13)$ to $R(10)$ transitions with a typical uncertainty of 0.40 MHz. These measurements improve previously known transition frequencies by at least an order of magnitude.

1. Introduction

Methane is a historically important molecule of study for scientists in many fields. Methane provided a fundamental guidepost for understanding molecular geometry and chemical bonding [1]. As the simplest stable hydrocarbon, methane has been and continues to be a key benchmark for molecular modeling and state-of-the-art *ab initio* calculations of potential energy and dipole moment surfaces [2,3]. Modern *ab initio* work is useful for predicting line strengths and supplementing incomplete experimental spectra, which can contribute to spectroscopic linelists like the HITRAN database [4]. Similarly, methane is relevant to the ExoMol project, which is focused on creating accurate astrophysical models of cool stars and extrasolar planets [5], since methane is a key constituent of planetary atmospheres [6,7] and brown dwarf atmospheres [8]. Here on Earth, methane is the third most abundant greenhouse gas and therefore a significant contributor to climate change [9], as well as being relevant to ozone depletion and formation [10].

Methane's rovibrational structure is best studied by mid-infrared spectroscopy due to its strong rovibrational transition dipole moments. However, its tetrahedral symmetry and overlap of normal mode frequencies for its four vibrational bands result in a highly complex vibrational structure. Specifically, the ν_1 and ν_3 bands consisting of C-H stretching vibrations have normal mode frequencies of roughly 3000 cm^{-1}, while the ν_2 and ν_4 bands consisting of C-H bending vibrations have normal mode frequencies of roughly 1500 cm^{-1} [11]. The vibrational bands of methane are grouped into polyads, which are named by the number of interacting bands, including fundamental, overtone, combination, and hot bands, in a given frequency region; the polyads increase in complexity with frequency, making assignment and analysis of the near-infrared and above very difficult.

The pentad region ($\nu_1, \nu_3, \nu_2+\nu_4, 2\nu_2, 2\nu_4$; 2300–3300 cm^{-1}) has been modeled with high accuracy in the past [2,3,12,13]. Agreement between theory and experiment now surpasses 0.1 cm^{-1} in the pentad region [2], and will likely soon surpass Doppler-limited precision. In order to continue to provide accurate benchmarks for *ab initio* calculations, line centers must be determined to sub-Doppler uncertainty. Moreover, methane is worth revisiting now due to the advent of more sophisticated techniques and widely tunable high-power mid-infrared light sources during the past few decades, which allow for much higher precision and accuracy in determining line centers.

Sub-Doppler spectroscopy overcomes the limitation of Doppler broadening from traditional spectroscopy. One method of performing sub-Doppler spectroscopy involves the use of a double-pass configuration, where the incident beam serves to saturate the transition, and the reflected beam probes the change in population. When a transition is saturated, a narrow dip in the absorption of the reflected beam is observed. This feature, known as a Lamb dip, is centered at the transition frequency, since it occurs when

* Corresponding author.
E-mail address: bjmccall@illinois.edu (B.J. McCall).
[1] Current address: Cymer, Inc., 17075 Thornmint Court, San Diego, CA 92127, USA.

https://doi.org/10.1016/j.jqsrt.2018.04.033
0022-4073/

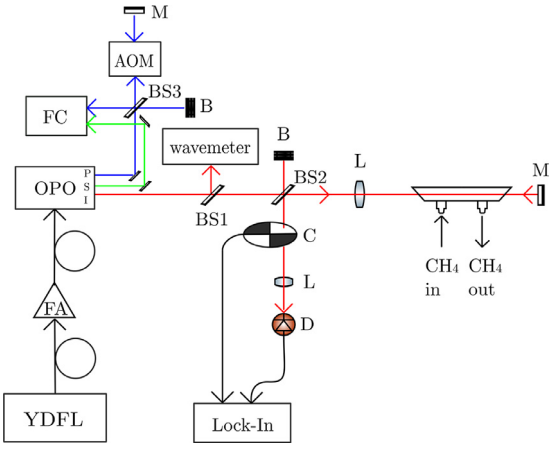

Fig. 1. Experimental layout. YDFL: ytterbium-doped fiber laser, FA: fiber amplifier, OPO: optical parametric oscillator, BS1: 99/1 beamsplitter, BS2: 50/50 beamsplitter, B: beam block, L: lens, M: back-reflecting mirror, C: beam chopper, D: detector, BS3: 70/30 beamsplitter, AOM: acousto-optic modulator, and FC: frequency comb.

the counter-propagating beams interact with the same molecules, thereby overcoming Doppler broadening. Lamb dip widths are also roughly two orders of magnitude narrower than a traditional Doppler-broadened profile, since Lamb dips are limited only by the homogeneous line width. When combined with the highly stable frequency calibration provided by an optical frequency comb, sub-Doppler spectroscopy allows for precise and accurate determination of transition frequencies.

The ν_3 band of methane has been studied quite extensively in Doppler-limited surveys using Fourier transform infrared (FTIR) spectroscopy [13–15] with uncertainties ranging from 3 to 300 MHz and dual-comb spectroscopy [16] where sub-MHz uncertainties were achieved. More recently, several groups have turned to saturation using difference frequency generation sources to perform sub-Doppler spectroscopy with high precision [17,18]. By stabilizing the frequency of the source to saturated absorption lines [19], transitions were recorded with uncertainties of 4–40 kHz. One large-scale sub-Doppler survey performed with cavity enhancement [20,21] covered a total of 204 lines with a typical uncertainty of 3 kHz for allowed transitions and 12 kHz for forbidden transitions, which were observed with wavelength modulation. However, many fairly strong transitions in the pentad region are still known to relatively high uncertainty, which we aim to ameliorate. Here, as an extension of the sub-Doppler work on the ν_3 band of methane [19–21], we report 22 methane transitions in the pentad region with uncertainties improved by at least an order of magnitude [4,13,14,22].

2. Experimental

A diagram of the instrument is shown in Fig. 1. 1064 nm light from an ytterbium-doped fiber laser (Koheras Adjustik Y10) is sent to an erbium-doped fiber amplifier (IPG Photonics YAR-10K-1064-LP-SF), which amplifies the light to 8 W. The amplified light is sent to an optical parametric oscillator (OPO; Aculight Argos 2400 SF) to generate idler (400 mW, 3.2–3.9 µm) and signal beams via parametric down-conversion. The idler beam is sent through a 40 cm glass flow cell filled with 75–470 mTorr of $^{12}CH_4$, and is reflected back through the cell. The reflected beam is picked off by a 50/50 Si beamsplitter, modulated by a beam chopper, and focused on a fast mid-infrared photodiode detector (Boston Electronics Vigo, PVM-10.6). The detector output is sent to a lock-in amplifier referenced by the frequency of the chopper. The scans shown here were recorded with a 0.1 MHz step size and a 300 ms time constant.

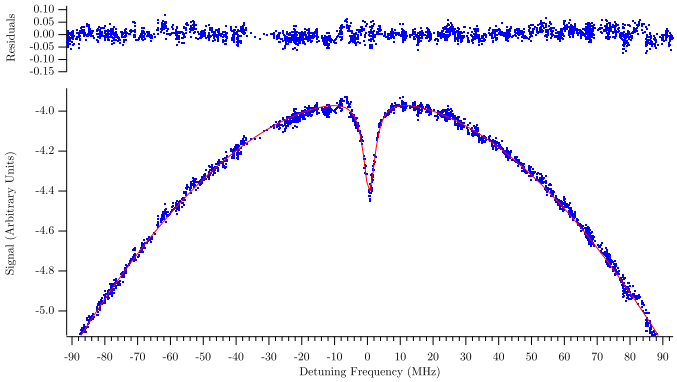

Fig. 2. A representative scan of the F_2 component of the $Q(3)$ transition, centered at 90,488,114 MHz. The dots are the data points, and the curve is the fit. The dots plotted above are the residuals of the fit. The width of the Lamb dip is 4.18 MHz (FWHM).

Frequency calibration of the idler is derived from the difference of the pump and signal frequencies ($\nu_{idler} = \nu_{pump} - \nu_{signal}$), which are calibrated with an optical frequency comb (Menlo Systems FC-1500; 100 MHz repetition rate). An infrared wavemeter (Bristol 621:IR-A) is used for crude frequency calibration and to help determine the number of comb modes between the pump and signal frequencies. The signal beam is locked at an offset of 20 MHz to a single comb tooth via a phase-locked loop, with corrections sent to a piezoelectric transducer (PZT) on the signal cavity within the OPO.

The pump beat is kept within the 25–35 MHz internal bandpass of a frequency counter with a feed-forward mechanism using a freespace acousto-optic modulator (AOM; Brimrose IPF-200-80-1600) in a double-pass configuration using a 70/30 beamsplitter. The idler is stepped by incrementing the voltage sent to the seed laser's PZT by an amount which corresponds to a 0.1 MHz shift in frequency. The AOM then applies a correction to the pump to re-center it within the bandpass of the frequency counter, which is calculated by the acquisition software. The frequency counter reads the beat note frequency, and if it is not in the center of the bandpass, additional AOM corrections are made. Once the beat is centered, a data point is acquired, and the voltage is then stepped again to collect another data point. When the AOM reaches the edge of its diffraction efficiency, the frequency is either increased or decreased accordingly by 50 MHz to create a 100 MHz shift to the next comb tooth. Each point was collected after a 1.5 s delay to allow the frequency counters to update.

3. Results and discussion

A representative scan is shown in Fig. 2, which is the F_2 component of the $Q(3)$ transition of the ν_3 band. Transitions typically had Doppler widths of approximately 400 MHz (full width at half maximum, FWHM) and Lamb dip widths of approximately 4.5 MHz (FWHM). This is attributed to a combination of pressure broadening, power broadening, transit-time broadening, and broadening from the spectral linewidth of the laser. As an example, in the case of the F_2 component of the $Q(3)$ transition, the self-broadening coefficient for the $J'' = 3$ state is estimated to be 0.079 cm^{-1}/atm [23] (half width at half maximum, HWHM), or 6.23 MHz/Torr (FWHM). Pressures of 75–470 mTorr translate to widths of 0.4-2.4 MHz. The Einstein A coefficient for this transition is estimated to be 24.7 Hz [4], giving a transition dipole moment of ~0.054 D. The incident beam had a power of about 200 mW with a beam waist of about 0.32 mm, translating to power broadening of about 1 MHz. Transit-time broadening was estimated to be 0.9 MHz. Broadening from the spectral linewidth of the radia-

Table 1
A comparison between the new measurements and previous measurements of transitions in the ν_3 band of $^{12}CH_4$. Uncertainties are represented by σ, and the difference (new–previous) is represented by δ.

Trans.	Comp.	Meas. Freq. (MHz)	σ (MHz)	Prev. Freq. (MHz)	Prev. σ (MHz)	δ (MHz)
$P(4)$	A_1	89 308 512.47	0.24	89 308 512.256 8[a]	0.002 0	0.21
$P(3)$	A_2	89 601 828.50	0.32	89 601 828.651 4[a]	0.002 5	−0.15
$Q(8)$	$F_2^{(1)}$	90 411 883.95	0.23	90 411 883.753 6[b]	0.003 5	0.20
$Q(8)$	$E^{(2)}$	90 426 451.01	0.14	90 426 450.987 8[b]	0.002 5	0.02
$Q(8)$	$F_2^{(2)}$	90 428 470.18	0.21	90 428 470.084 7[b]	0.003 0	0.09
$Q(3)$	F_1	90 484 623.26	0.16	90 484 623.067 9[a]	0.002 0	0.19
$Q(3)$	F_2	90 488 114.50	0.14	90 488 114.363 3[a]	0.002 0	0.14
$Q(3)$	A_2	90 493 215.45	0.14	90 493 215.526 8[a]	0.002 1	−0.07
$Q(2)$	E	90 495 092.46	0.22	90 495 092.106 1[a]	0.002 3	0.35
$Q(2)$	F_2	90 496 856.61	0.24	90 496 856.544 3[a]	0.002 0	0.07
$Q(1)$	F_1	90 502 080.65	0.33	90 502 080.707 9[a]	0.002 1	−0.05
$R(0)$	A_1	90 799 708.521	0.086	90 799 708.460 6[b]	0.003 5	0.06
$R(5)$	$F_1^{(2)}$	92 232 637.74	0.33	92 232 637.852 8[b]	0.003 5	−0.11
$R(5)$	F_2	92 236 455.46	0.13	92 236 455.591 8[b]	0.003 4	−0.13

[a] Okubo et al. [20].
[b] Abe et al. [21].

Table 2
Measured transition frequencies of the ν_3 band of $^{12}CH_4$. Uncertainties are represented by σ, and the difference (new–previous) is represented by δ.

Trans.	Comp.	Meas. Freq. (MHz)	σ (MHz)	Prev. Freq. (MHz)	Prev. σ (MHz)	δ (MHz)
$P(13)$	A_2	86 492 798.43	0.20	86 492 824[a]	18	−25.3
$P(13)$	A_1	86 512 941.30	0.30	86 512 934[a]	18	7.1
$Q(13)$	$E^{(1)}$	90 264 009.38	0.63	90 264 003[a]	18	6.6
$Q(13)$	$F_1^{(3)}$	90 292 115.52	0.57	90 292 103[a]	18	12.5
$Q(13)$	$E^{(2)}$	90 315 521.4	1.3	90 315 545[a]	30–300[b]	−23.6
$R(9)$	A_2	93 333 228.93	0.46	93 333 232[a]	18	−3.1
$R(9)$	$F_2^{(2)}$	93 333 782.03	0.15	93 333 780[a]	18	2.3
$R(9)$	$F_1^{(3)}$	93 334 428.42	0.74	93 334 421[a]	18	7.6
$R(9)$	A_1	93 336 791.20	0.14	93 336 792[a]	18	−1.3
$R(9)$	$F_1^{(2)}$	93 337 911.61	0.18	93 337 906[a]	18	5.9
$R(9)$	E	93 338 231.72	0.31	93 338 231[a]	18	1.0
$R(9)$	$F_2^{(1)}$	93 346 602.15	0.40	93 346 597[a]	18	5.1
$R(9)$	$F_1^{(1)}$	93 346 738.59	0.60	93 346 735[a]	18	3.3
$R(10)$	$F_2^{(3)}$	93 602 932.75	0.54	93 602 925[c]	3–30[d]	7.7
$R(10)$	$E^{(2)}$	93 603 751.27	0.46	93 603 759[e]	3	−7.6
$R(10)$	$F_1^{(2)}$	93 604 085.42	0.15	93 604 085[a]	18	0.2
$R(10)$	A_1	93 605 158.06	0.25	93 605 147[a]	18	11.4
$R(10)$	$F_1^{(1)}$	93 608 383.63	0.37	93 608 375[f]	17	9.0
$R(10)$	$F_2^{(2)}$	93 608 521.59	0.44	93 608 516[f]	17	6.0
$R(10)$	A_2	93 618 091.33	0.12	93 618 065[a]	18	26.2
$R(10)$	$F_2^{(1)}$	93 618 121.80	0.19	93 618 105[a]	18	16.6
$R(10)$	$E^{(1)}$	93 618 132.90	0.34	93 618 131[e]	3	1.7

[a] Daumont et al. [14].
[b] Uncertainty index 3 from the HITRAN2016 database [4].
[c] Gordon et al. [4].
[d] Uncertainty index 4 from the HITRAN2016 database [4].
[e] Albert et al. [13].
[f] Tyuterev et al. [22].

tion from the laser was estimated to be 0.5 MHz by observing the widths of the beats generated by the pump and signal beams with the modes of the frequency comb.

In order to verify the efficacy of the spectrometer and the accuracy of the calibration, we measured 14 transitions which had already been measured to kHz-level uncertainty. Table 1 shows the comparison of the 14 measured lines between our values and the literature values [20,21]. Lines were measured at least five times, using the arithmetic mean of the values as the center and the sample standard deviation of the set of transition frequencies as the uncertainty. In each case, our measured value agrees with the literature value within twice our standard deviation, with the majority within one standard deviation, lending reliability to the method.

Table 2 lists the 22 measured transition frequencies with their uncertainties in MHz, the previously measured frequencies as listed in the HITRAN2016 database [4,13,14,22], and the differences between the two. Lines were measured at least seven times on at least two separate days. The data have an average uncertainty of 0.40 MHz, ranging from 0.12 MHz to 1.3 MHz, with higher uncertainties generally accompanying weaker transitions. All newly measured frequencies agree with past measurements within 2σ with the exception of the $E^{(2)}$ component of the $R(10)$ transition as reported by Albert et al. [13], which was a Doppler-broadened experiment. Other transitions from this work have been remeasured in a sub-Doppler survey by Abe et al. [21], where disagreements were well outside of the reported Doppler-broadened uncertainty of $\sim$3 MHz for transitions within the pentad region.

Scans were fit by modeling the Lamb dip as a Lorentzian lineshape and the Doppler profile as a Gaussian lineshape. In the instances of multiple overlapping Doppler profiles, fitting functions were adjusted accordingly to the number of transitions which were measured. For example, the A_2, $F_2^{(1)}$, and $E^{(1)}$ components of the

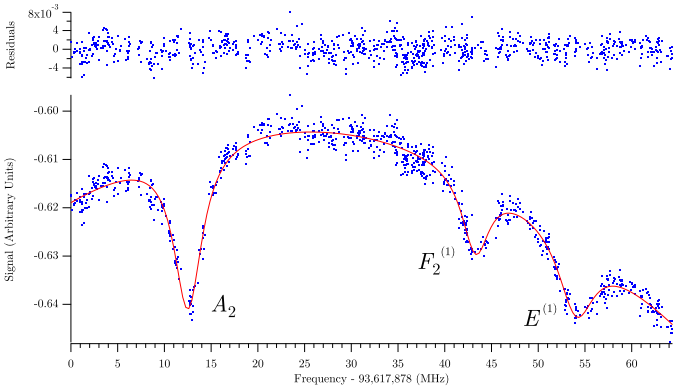

Fig. 3. A scan of the A_2, $F_2^{(1)}$, and $E^{(1)}$ components of the $R(10)$ transition, relative to 93,617,878 MHz. The dots are the data, the curve is the fit, and the dots plotted above show the residuals.

$R(10)$ transition shown in Fig. 3 were fit simultaneously as a sum of three Lorentzian profiles with three accompanying Gaussian profiles.

4. Conclusion

We have measured 22 transitions in the pentad region of methane. All transitions were measured to MHz-level uncertainty by taking advantage of the narrow sub-Doppler features resulting from saturated absorption. These values improve the precision of known transition frequencies by at least an order of magnitude. This work can be used for more precise modeling of methane as a benchmark for new *ab initio* calculations.

Funding

P.A.K. is grateful for funding from the University of Illinois at Urbana-Champaign Campus Honors Program Summer Research Grant, and for financial support from a Peter C. & Gretchen Miller Markunas Scholarship and a Matthews Scholarship. C.R.M. is grateful for support from a National Aeronautics and Space Administration (NASA) Earth and Space Science Fellowship (NESSF NNX16AO86H). This work was also funded by a grant from the National Science Foundation (NSF PHY 14-04330).

Conflicts of interest

None.

References

[1] Pauling L. The nature of the chemical bond. Application of results obtained from the quantum mechanics and from a theory of paramagnetic susceptibility to the structure of molecules. J Am Chem Soc 1931;53(4):1367–400. doi:10.1021/ja01355a027.

[2] Nikitin AV, Rey M, Tyuterev VG. Accurate line intensities of methane from first-principles calculations. J Quant Spectrosc Radiat Transf 2017;200:90–9. doi:10.1016/j.jqsrt.2017.05.023.

[3] Nikitin AV, Rey M, Tyuterev VG. First fully *ab initio* potential energy surface of methane with a spectroscopic accuracy. J Chem Phys 2016;145:114309. doi:10.1063/1.4961973.

[4] Gordon IE, Rothman LS, Hill C, Kochanov RV, Tan Y, Bernath PF, et al. The HITRAN2016 molecular spectroscopic database. J Quant Spectrosc Radiat Transf 2017;203:3–69. doi:10.1016/j.jqsrt.2017.06.038.

[5] Tennyson J, Yurchenko SN, Al-Refaie AF, Barton EJ, Chubb KL, Coles PA, et al. The ExoMol database: molecular line lists for exoplanet and other hot atmospheres. J Mol Spectrosc 2016;327:73–94. doi:10.1016/j.jms.2016.05.002.

[6] Owen T, Cess RD. Methane absorption in the visible spectra of the outer planets and Titan. Astrophys J 1975;197:L37–40. doi:10.1086/181771.

[7] Swain MR, Vasisht G, Tinetti G. The presence of methane in the atmosphere of an extrasolar planet. Nature 2008;452:329–31. doi:10.1038/nature06823.

[8] Oppenheimer BR, Kulkarni SR, Matthews K, van Kerkwijk MH. The spectrum of the brown dwarf Gliese 229B. Astrophys J 1998;502(2):932–43. doi:10.1086/305928.

[9] Khalil MAK. Non-CO_2 greenhouse gases in the atmosphere. Annu Rev Energy Environ 1999;24(1):645–61. doi:10.1146/annurev.energy.24.1.645.

[10] Boucher O, Friedlingstein P, Collins B, Shine KP. The indirect global warming potential and global temperature change potential due to methane oxidation. Environ Res Lett 2009;4(4):044007. doi:10.1088/1748-9326/4/4/044007.

[11] Gray DL, Robiette AG. The anharmonic force field and equilibrium structure of methane. Mol Phys 1979;37(6):1901–20. doi:10.1080/00268977900101401.

[12] Hilico JC, Champion JP, Toumi S, Tyuterev VG, Tashkun SA. New analysis of the pentad system of methane and prediction of the (pentad-pentad) spectrum. J Mol Spectrosc 1994;168(2):455–76. doi:10.1006/jmsp.1994.1293.

[13] Albert S, Bauerecker S, Boudon V, Brown LR, Champion J-P, Loëte M, et al. Global analysis of the high resolution infrared spectrum of methane $^{12}CH_4$ in the region from 0 to 4800 cm^{-1}. Chem Phys 2009;356(1–3):131–46. doi:10.1016/j.chemphys.2008.10.019.

[14] Daumont L, Nikitin AV, Thomas X, Régalia L, Von der Heyden P, Tyuterev VG, et al. New assignments in the 2 µm transparency window of the $^{12}CH_4$ octad band system. J Quant Spectrosc Radiat Transf 2013;116:101–9. doi:10.1016/j.jqsrt.2012.08.025.

[15] Féjard L, Champion JP, Jouvard JM, Brown LR, Pine AS. The intensities of methane in the 3–5 µm region revisited. J Mol Spectrosc 2000;201:83–94. doi:10.1006/jmsp.2000.8065.

[16] Baumann E, Giorgetta FR, Swann WC, Zolot AM, Coddington I, Newbury NR. Spectroscopy of the methane ν_3 band with an accurate midinfrared coherent dual-comb spectrometer. Phys Rev A 2011;84(6):062513. doi:10.1103/PhysRevA.84.062513.

[17] Maddaloni P, Gagliardi G, Malara P, De Natale P. A 3.5-mW continuous-wave difference-frequency source around 3 µm for sub-Doppler molecular spectroscopy. Appl Phys B 2005;80(2):141–5. doi:10.1007/s00340-004-1714-0.

[18] Anzai K, Gao X, Sasada H, Yoshida N. Narrow lamb dip of 3.4 µm band transition of methane with difference frequency generation and enhancement cavity. Jpn J Appl Phys 2006;45(4A):2771–5. doi:10.1143/JJAP.45.2771.

[19] Takahata K, Kobayashi T, Sasada H, Nakajima Y, Inaba H, Hong F-L. Absolute frequency measurement of sub-Doppler molecular lines using a 3.4-µm difference-frequency-generation spectrometer and a fiber-based frequency comb. Phys Rev A 2009;80:032518. doi:10.1103/PhysRevA.80.032518.

[20] Okubo S, Nakayama H, Iwakuni K, Inaba H, Sasada H. Absolute frequency list of the ν_3-band transitions of methane at a relative uncertainty level of 10^{-11}. Opt Express 2011;19(24):23878–88. doi:10.1364/OE.19.023878.

[21] Abe M, Iwakuni K, Okubo S, Sasada H. Accurate transition frequency list of the ν_3 band of methane from sub-Doppler resolution comb-referenced spectroscopy. J Opt Soc Am B 2013;30(4):1027–35. doi:10.1364/JOSAB.30.001027.

[22] Tyuterev V, Tashkun S, Rey M, Kochanov R, Nikitin A, Delahaye T. Accurate spectroscopic models for methane polyads derived from a potential energy surface using high-order contact transformations. J Phys Chem A 2013;117(50):13779–805. doi:10.1021/jp408116j.

[23] Brown LR, Sung K, Benner DC, Devi VM, Boudon V, Gabard T, et al. Methane line parameters in the HITRAN2012 database. J Quant Spectrosc Radiat Transf 2013;130:201–19. doi:10.1016/j.jqsrt.2013.06.020.